Comparative study on the hydrogenation of naphthalene over both Al_2O_3 supported Pd and NiMo catalysts against a novel LDH-derived Ni-MMO-supported Mo catalyst

Claydon, Ryan; Roman Ramirez, Luis; Wood, Joe

DOI:
10.1021/acsomega.1c03083

Document Version
Publisher's PDF, also known as Version of record

Citation for published version (Harvard):
Claydon, R, Roman Ramirez, L & Wood, J 2021, 'Comparative study on the hydrogenation of naphthalene over both Al_2O_3 supported Pd and NiMo catalysts against a novel LDH-derived Ni-MMO-supported Mo catalyst', *ACS Omega*, vol. 6, no. 30, pp. 20053-20067. https://doi.org/10.1021/acsomega.1c03083

Comparative study on the hydrogenation of naphthalene over both Al_2O_3-supported Pd and NiMo catalysts against a novel LDH-derived Ni-MMO-supported Mo catalyst

Ryan M. Claydon; Luis A. Roman-Ramirez; Joseph Wood*

RXC095@bham.ac.uk*

School of Chemical Engineering, University of Birmingham, Edgbaston, Birmingham, B15 2TT, U.K.

Abstract

Naphthalene hydrogenation was studied over a novel Ni-Al layered double hydroxide-derived Mo-doped mixed metal oxide (Mo-MMO), contrasted against bifunctional $NiMo/Al_2O_3$, and Pd-doped Al_2O_3 catalysts, the latter of which with Pd loadings of 1, 2 and 5 wt%. Reaction rate constants were derived from a pseudo-first order kinetic pathway describing a two-step hydrogenation pathway to tetralin (k_1) and decalin (k_2). The Mo-MMO catalyst achieved comparable reaction rates to $Pd_{2\%}/Al_2O_3$ at double concentration. When using $Pd_{5\%}/Al_2O_3$, tetralin hydrogenation was favored over naphthalene hydrogenation culminating in a k_2 value of 0.224 compared to a k_1 value of 0.069. The Ni and Mo-based catalysts produced the most significant cis-decalin production, with Mo-MMO culminating at a cis/trans ratio of

0.62 as well as providing enhanced activity in naphthalene hydrogenation compared to $NiMo/Al_2O_3$. Consequently, Mo-MMO presents an opportunity to generate more alkyl naphthenes in subsequent hydrodecyclisation reactions and therefore a higher cetane number in transport fuels. This is contrasted by a preferential production of trans-decalin observed when using all of the Al_2O_3-supported Pd catalysts, as a result of the octalin intermediate orientations on the catalyst surface as a function of the electronic properties of Pd catalysts.

1. Introduction

Polyaromatic Hydrocarbons (PAH) comprise the organic group containing two or more aromatic rings bonded together. These compounds represent a deleterious fraction in hydrocarbon fuels, leading to an incomplete combustion and consequently soot production, in addition to a reduction of the cetane number in diesel fuels [1]. Environmental legislation is turning towards ever more stricter guidelines that include reducing such compounds [2]. These compounds are prevalent in lower quality heavy oils. A unique conceptualization of the In Situ Combustion (ISC) process utilizes a horizontal well with catalyst pellets packed in the annular space. This is known as the Toe-to-Heel Air Injection and Catalytic Process In-situ process (THAI-CAPRI) [3], which has the potential to emanate refinery units such as primary and secondary stage hydrotreating reactors given the complex temperature zones up to 450 ℃. This is particularly relevant at lower temperatures observed under the wet-mode ISC conditions in addition to thermal EOR mechanisms such as In Situ Upgrading Technology (ISUT) which generates fields of temperature zones reaching 320 ℃ [4,5]. Notwithstanding this, at the higher end of the temperature range, it has been shown by Chong et al [6] that monoaromatic and cycloalkane production is favored. However, identifying a material which could adequately refine or remove PAH compounds at a relatively price competitive margin promotes further investigation into the use of this technology.

Hydrogenation studies have previously focused on a great variety of catalytic materials. Noble metals have demonstrated the most significant rates of hydrogenation, however, the expense of the materials has led to the focus on transition metal-based catalysts [7]. Many forms have been used in hydrogenation reactions including carbides, phosphides, oxides, nitrides and sulfides [8–10].

While the PAH components in heavy oil typically involve very complex molecules, the use of a model compound such as naphthalene is useful to understand the selectivity and pathways governing polyaromatic group hydrogenation [11]. Tetrahydronaphthalene (tetralin), a hydrogenated derivative of naphthalene, has been used previously to represent deleterious aromatics in fuel feeds [12]. Hydrogenation of this molecule leads to- the formation of both cis- and trans-decahydronaphthalene (decalin) via the intermediate pathway involving octahydronaphthalene ($\Delta^{1,9}$ – octalin). These two products, however, comprise contrasting reactivities to ring-opening and ring-contraction.

Cis-decalin is far less thermodynamically stable, which results in greater selectivity to ring-opening reactions via selective hydrodecyclization [13]. This conversion process results in the production of alkylated single-ring naphthenes, from multi-ting naphthene precursors such as decalin, generating an improved cetane number [14]. Consequently, this justifies the effort to maintain a high cis/trans -decalin ratio. In previous works, the impact of tetralin concentration on the cis/trans ratio was shown to be negligible until most of the tetralin had undergone hydrogenation [15]. Upon reaching the high conversion, the cis/trans ratio approached an equilibrium. It was suggested that the competition for catalytic adsorption sites was responsible for inhibiting cis to trans isomerization up until significant tetralin conversion. Wang et al. [16] synthesized a chromium-based Metal Organic Framework (MOF) for use in tetralin hydrogenation reactions spanning 140 to 220 ℃ across a range of 30 to 70 bar H_2. The results

indicated that a highly enriched cis/trans ratio was achieved across all levels of tetralin conversion, due to a greater adsorption facility for tetralin by the highly porous MOF support.

The choice of catalytic material is important as it can significantly affect the adsorption and dissociation energy barriers required for hydrogen activation and subsequent hydrogenation of the target molecule [17]. Previous studies have examined the effect of hydrogen activation of individual Pd atom surface sites and the impact of particle size and dispersion on observed chemistry. A study conducted by Yu et al. [18] summarized the beneficial impact of contiguous Pd active sites over a bimetallic catalyst, facilitating a greater dissociative adsorption of hydrogen over a bimetallic catalyst. It was suggested that the contiguous Pd sites could be retained through either heat treatment or depositing a greater coverage of Pd. It has been found that when embedding Pd into Au, monomers are prevalent at lower coverages while an increased coverage generates clusters of Pd which can have an impact on dissociation, spillover and desorption of hydrogen [17].

Many noble metal-based catalytic studies focus on second-stage hydrotreating (HDT) and hydrogenation (HYD) reactions deposited over protonic supports [19–21]. This includes Al_2O_3-supported platinum and palladium catalysts [15]. This electron-deficiency, however, can result in over-cracking and an overproduction of coke and catalyst deactivation. This can be mitigated by using more neutral supports such as silica-alumina supported noble metals or non-acidic supports [22–26]. Works using supports such as zirconium-doped mesoporous silica have been used in the hydrogenation of tetralin, highlighting very active catalysis at 350 ℃ and 6.0 MPa hydrogen pressure [27]. Research has also recently been undertaken to assess the impact of both noble and group VI metals over basic carriers in both HYD and hydrodesulfurization (HDS) reactions [13,28–31]. It has been shown that a 2 wt.% concentration of alkaline-earth metals dispersed over the conventional acidic support led to greater activity of the platinum during the hydrogenation reaction of naphthalene [13]. The works in Escobar et al. [13] added to previous

experimental work wherein basic supports were investigated and hypothesized to interact with the metallic Ru nanoparticles, producing dual-site heterolytic hydrogen splitting and surface ionic hydrogenation pathways [30]. Bimetallic Pd-Pt catalysts supported by Mg-Al mixed oxide was also synthesized to assess its activity for hydrogenation and hydrogenolysis of high molecular weight compounds as well as its thio-resistance, a necessary property given the presence of S-containing compounds in hydrotreated feeds [32]. The results indicated that the catalyst exhibited high activity to decalin production, however, upon decreasing the Pd/Pt ratio the hydrogenation products decreased while the role of Pt-catalyzed hydrogenolysis reactions increased. Furthermore, hydrogenolysis reactions did not contribute to the formation of tar which was in turn attributed to the lack of strong Brønsted acid sites exhibited by the basic mixed oxide support. Previous works have adopted a pseudo first order kinetic constant regime with respect to naphthalene concentration during the comparison of the catalysts [13,26].

Previous studies [12,13,15,23] have generated encouraging results which have prompted an assessment of whether a novel Mo-doped Ni-enriched Mixed Metal Oxide (Mo-MMO) could provide an economical alternative to naphthalene hydrogenation, a compound used to represent deleterious compounds found in heavier oil reservoirs and thereby directed for refinement in first and second-stage HDT and HDA units. Layered Double Hydroxides (LDH)-derived mixed metal oxides (MMOs) have been largely studied in the literature in various reactions, owing to their tunability, resulting in variations in electronic configuration, dispersion and surface area and reducibility, which have fundamental impacts on their performance as catalysts [33,34]. Furthermore, the synthesis of LDHs remains an inexpensive alternative to typical highly tuned supports, due to the relative ease of coprecipitation and the ability to use a variety of waste streams for metal salt precursors [35,36]. The MMOs that are obtained following LDH heat treatment generate a high surface area, homogenous solid solution of oxides which can have shown to be appropriate catalytic supports for HDT reactions [37].

This study uniquely explores the possibility of using Ni-enriched, LDH-derived MMOs as supports doped with Mo using the incipient wetness impregnation technique. The reaction rate constant kinetic parameters from batch reactor experiments are constrained and contrasted against typical refinery grade Ni, Mo and Pd-bearing catalysts on two-step naphthalene hydrogenation to tetralin and decalin. A comparison of cis/trans-decalin ratios is made as a function of tetralin conversion during the hydrogenation reaction highlighting the apparent differences between the metal classes and both basic and acidic-enriched support materials introduced into the reaction. An assessment is made to understand how effectively the catalysts can generate the compound, cis-decalin, which is more easily upgraded during further hydrodecyclisation treatment.

2. Experimental

2.1 Catalyst synthesis

A Ni-enriched LDH was synthesized using the co-precipitation method. Two metal salts $Ni(NO_3)_2 \cdot 6H_2O$ and $Al(NO_3)_3 \cdot 9H_2O$, were added to distilled water in the appropriate molar ratios to reach a 3.3:1 Ni:Al ratio in a 0.3M 200mL. The metal salt solution was sequentially pumped into a second solution containing sodium carbonate adhering to the appropriate ratio $[CO_3^{2-}]/[M^{3+}] = 0.5$, to commence the in-situ formulation of anionic clay. A NaOH solution was used to control the pH to promote LDH precipitation in a pH range of 9 to 10 and a stirring speed was set at 500 rpm. Precipitation occurred over the period of 12 h at 60 ℃ to promote adequate crystallization.

Following this precipitation and crystallization procedure, the resultant LDH was washed with deionized water to remove impurities. The samples were subsequently calcined at 450℃ for 4 h using a heating ramp rate of 10 ℃ min^{-1}. Following this oxidation process, the resultant Ni-MMO was doped with Mo under incipient wetness impregnation in an excess of toluene. A

$MoCl_5$ (anhydrous) salt was added in the appropriate ratio to achieve 10 wt% Mo. This method was carried out under constant stirring and a temperature of 60℃ for 12 h. Upon completion of the Mo-impregnation, the resultant Mo-doped MMO was calcined in air at a temperature of 450℃ for 4 h using a ramp rate of 10 ℃ min-1, to remove any remaining impurities.

The Pd/Al2O3 catalysts are a pre-formulated series of industry catalysts containing 1 wt%, 2 wt% and 5 wt% Pd, defined in previous studies [38,39].

2.2 Catalyst Characterization

A Bruker D2 X-ray diffractometer (cobalt source and nickel filter) was used to generate Powder X-ray Diffraction (PXRD) patterns. The method included a scan speed of 30 min with a step size of 0.370 over a 2-theta range 10-100˚ to determine the atomic arrangement of the mineral crystals.

Changes to the catalyst structure as the temperature increased during calcination were analyzed using a NETZSCH TG 209 F1 to obtain a detailed Thermo-Gravimetric Analysis (TGA). The method required 22 mg of catalyst set into a platinum crucible, with a heating rate of 10 K min-1 from 25℃ to the maximum temperature of 900℃, under a constant flow set at 10 mL min-1 of air.

XRF was conducted on the sample using a S8 TIGER equipped with a high intensity 4 kW Rhodium X-ray tube, two collimators at 0.23° and 0.46° and five analyzer crystals. Confirmation of the elemental constituents following impregnation of the molybdenum species was obtained.

Brunauer-Emmett-Teller (BET) analysis was performed using a Micromeritics ASAP2020 at the University of Warwick. To sufficiently evacuate the pores in the catalysts, the degassing procedure involved heating the samples to 350℃ and holding for a duration of 6 hours.

Temperature Programmed Desorption (TPD), performed by University of Manchester, was used to evaluate the number of acid sites present in the catalyst, respectively. The method

included loading 20 mg of the catalyst into a quartz U-tube reactor and analyzing the sample using a Quantachrome ChemBet Pulsar equipped with a Thermal Conductivity Detector (TCD). The temperature ramp programme included room temperature to 900℃ at a rate of 10℃ min^{-1} while simultaneously recording the intensity of NH_3 5% uptake in He gas mix. Approximately 40 mg of the catalyst was heated under He to 300 ℃ prior to holding for the duration of 1 h and subsequently cooling to room temperature. The NH_3 5% gas mix was then introduced for 2 h, followed by the replacement of the He gas, and a ramping programme as before from room temperature to 900 ℃ under a 10 ℃ min^{-1} ramp rate.

The morphology of the catalysts was defined using Transmission Electron Microscopy (TEM), while the distribution of the active metal species in the catalysts was mapped using an Hitachi TM3030 Scanning Electron Microscopy (SEM) and Energy Dispersive X-ray spectrometer (EDS).

2.3 Naphthalene hydrogenation

The reaction was conducted in a 100 mL stainless steel Anton Parr batch reactor, conditions of which were chosen to reflect second-stage hydrotreating as use in previous work [13], at a fixed temperature of 250℃, a stirring speed of 1000 rpm, a H_2 atmosphere of 40 bar and catalyst to reactant ratio of 0.12g/0.18g, raising to 0.24g/0.18g with the Ni and Mo catalysts, while the synthesized Mo-MMO catalyst was also used in a single loading 0.12g/0.18g to investigate the cis and trans decalin relationship. The stirring speed was selected to eliminate diffusion limitations prevalent in the three-phase heterogeneous reaction and therefore ensure the experiments were under direct kinetic control. During the 20 min heating-up stage, a N2 atmosphere was added to prevent any reaction prior to the reaction temperature set-point of 250℃. At this temperature a 0.5mL vial was collected and analyzed to confirm the initial concentration of the reactants corresponded with the solution prior to heating. The N2 was

released and H2 at 40 bar was added to the reaction vessel. This was denoted as the time for reaction commencement. Liquor from the reaction was collected in vials at 20 min intervals for a 2 h period. The progression of the reaction was measured while the rate constants, k1 and k2 were derived reaction using a pseudo-first order kinetic model. The pressure was maintained at 40 bar and each vial collected represented a homogenous solution of suspended catalyst, reactant and product compounds at each time point.

All liquid samples were filtered using a micromembrane to remove the catalyst particles, generating a clear liquid. The residual samples were then analyzed using Agilent Technologies 6890N GC with a corresponding 7683 B Series injector. An Agilent 19091J-413 capillary column (nominal length, diameter and film thickness at 30.0m, 320.0 μm and 0.25 μm, respectively) was used accompanied with the following method: equilibration time of 3 min, with a ramp from 80℃ to 135℃ over 9 min and second stage to 300 ℃ over 4 min. The components were separated according to boiling point. The identified reaction products included first and second stage hydrogenation products, tetralin, cis decalin and trans decalin, respectively. Five-point calibrations were made both isolated in the solvent and in the presence of the other products/reactants, to ensure no complications were prevalent in the analysis of reactant and product mixtures.

3. Results and Discussion

3.1 Catalyst characterization

3.1.1 LDH thermal degradation

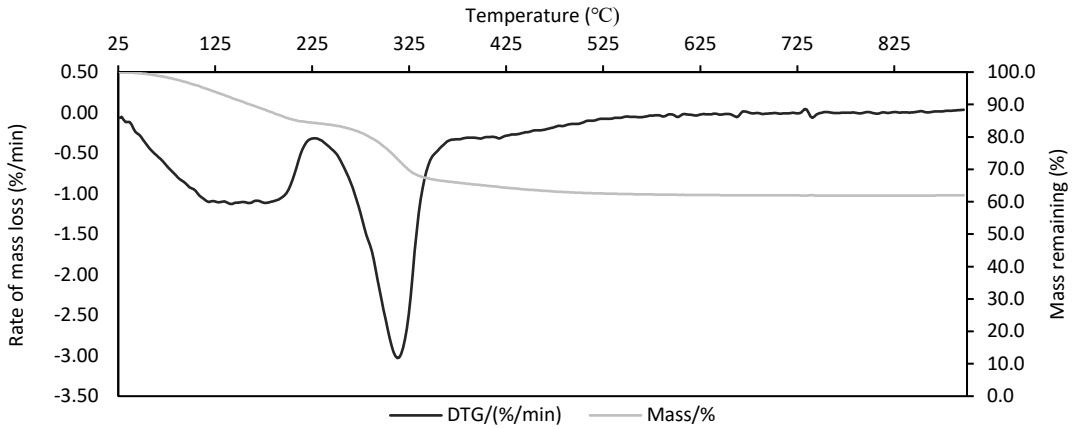

Figure 1. TGA profile of the nickel-enriched LDH, highlighting mass loss peaks corresponding to the structural properties of the material.

Thermogravimetric analysis of the synthesized nickel-enriched anionic clay highlights the process of MMO formation. The mass loss was measured as a function of time. Figure 1 highlights two distinctive peaks representing zones of mass loss which can be attributed to the loss of surface and interstitial water, in addition to interstitial decarboxylation and dehydroxylation of the metal hydroxide layers, respectively. This transition is in agreement with the literature [40], subsequently, resulting in a calcination process which produces a nickel-enriched metal oxide layer.

3.1.

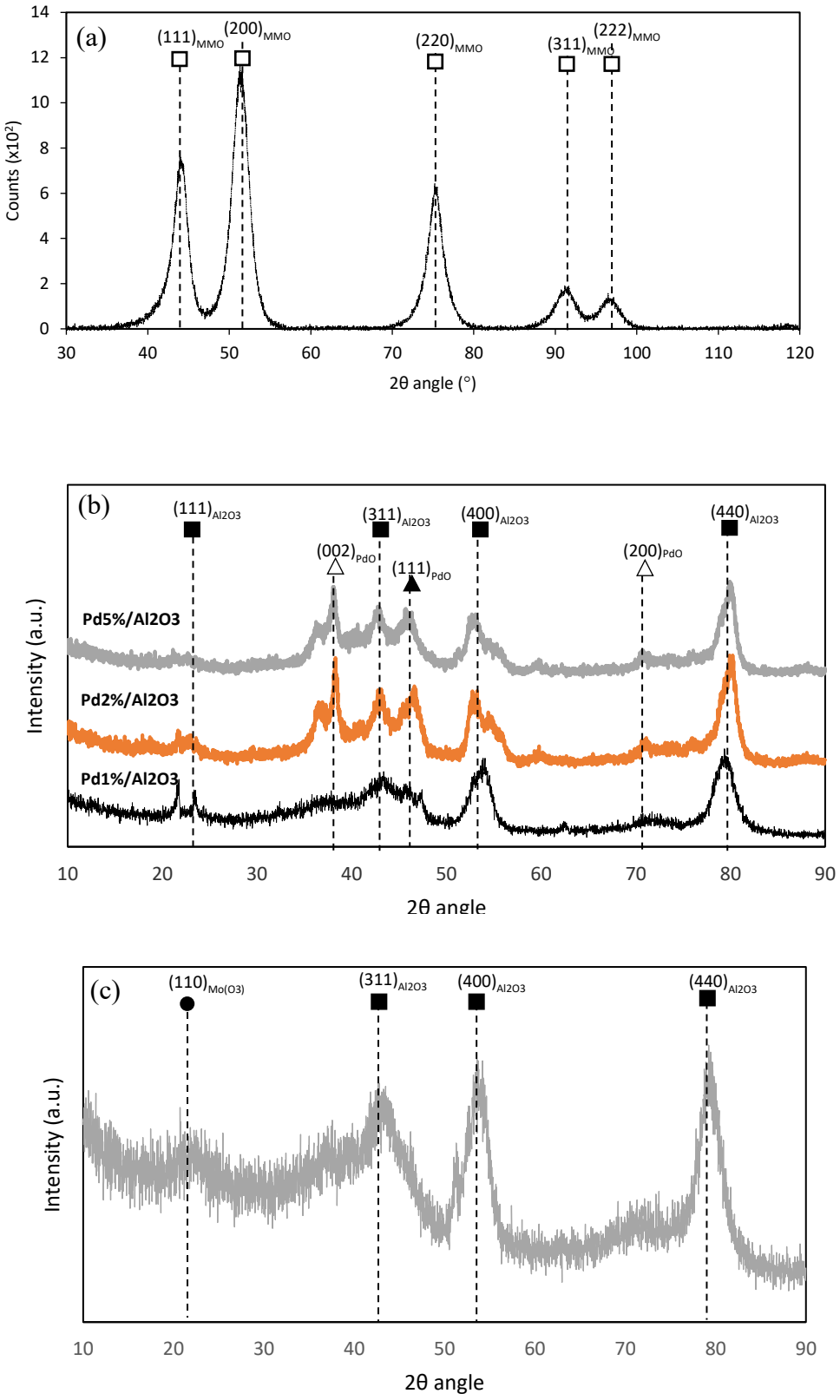

Figure 2. PXRD of (a) mixed oxides following calcination at 450 ℃, (b) $Pd_{1\%\text{-}5\%}$/alumina and (c) NiMo/alumina, the peaks of which are correlated to the 2 theta angles depicted in the figures.

The nickel-enriched anionic clay was subject to a calcination process at 450 °C. This was to ensure the material was completely delaminated forming high surface area polyphasic metal oxide sheets. The XRD pattern in Figure 2 (a) highlights the residual components of the material detailing peaks matched to the nickel oxide, Bunsenite mineral as recorded on Powder Diffraction File database, no. 00-047-1049, with corresponding peak indices (111), (200), (220), (311) and (222), from low to high 2θ, respectively. It is assumed that while poor crystallization has led to the absence of aluminium in the XRD profile, both quasi-amorphous spinel type and nickel-doped alumina phases can be found in the MMO.

The reflection peaks relating to the Al_2O_3 and PdO phases, present in all of the alumina-supported Pd catalysts illustrated in Figure 2(b), demonstrate the successive planes of (311), (400) and (440) and, (002) and (200), respectively, reported by JCPDS no. 10-0425. The $Pd_{1\%}/Al_2O_3$ species, however, presents poor indication of the PdO peaks indexed at (002), (111) and (200), in agreement with the lower concentration of Pd deposited over the Al_2O_3 support.

When analyzing the XRD diffraction pattern for $NiMo/Al_2O_3$, it is evident that the crystallization of the material is poor. However, the Al_2O_3 peaks of (311), (400) and (440) are clear, while the MoO_3 species present can be identified with the (110) peak. The nickel, however, is not observed due to its very small molar loading.

Table 1. Calculated molar ratios for the nickel and molybdenum catalysts using XRF analysis.

Element	Catalyst	
	Mo-MMO	NiMo/Al2O3
Ni	1.10	0.07
Al	0.33	1.25
Mo	0.09	0.09

The XRF results confirm the presence of a nickel-aluminium mixed oxide in a ratio of 3.3:1, with a 9 wt% loading of Mo, while the refinery catalyst demonstrates an enrichment of aluminium relating to the acidic alumina support accompanied by surface nickel impregnation on the same order as the molybdenum (Table 5.1).

3.1.3 Textural Properties

Table 2. Textural properties of the catalysts used in this study, derived from BET analysis.

	Mo-MMO	$NiMo/Al_2O_3$	$Pd_{1\%}/Al_2O_3$	$Pd_{2\%}/Al_2O_3$	$Pd_{5\%}/Al_2O_3$
Pore volume ($cc\ g^{-1}$)	0.39	0.67	0.48	0.63	0.38
Surface area ($m^2\ g^{-1}$)	141.62	220.58	186.88	119.15	110.37
Average pore size (Å)	54.5	60.7	51.3	10.6	69.7

The surface texture measurements of the catalysts are highlighted in Table 5.2. It is clear that the $NiMo/Al_2O_3$ demonstrates the highest surface area, coupled with the greatest pore volume and comparatively large pore size. When drawing comparisons with the LDH-derived catalyst, it is clear that the greater porosity and surface area observed over the $NiMo/Al_2O_3$ catalyst should theoretically provide for a higher activity in terms of upgrading larger components typically found in heavier oil feeds. When contrasting against the characterizations of the Pd-based catalysts, it is evident that while the $Pd_{5\%}/Al_2O_3$ is outperformed on pore volume and surface area, the average pore size is superior. This is a characteristic that will inhibit the coking of pore throats during upgrading of heavier feeds.

3.1.3 Acidity

The peaks of reduction and extent of NH_3 desorption across the temperature range 0-900^{o}C is shown in Figure 3 with the total acidity defined in Table 3.

NH_3 (5%)-TPD was performed to investigate the acidic properties of the catalyst. The peaks can be separated into three predominant groups, representing the strength of the acid site. As temperature increases, the strength of the acid site increases, generating bands of weak, medium and strong acid sites, the temperature ranges of which follow the approximation 100-200℃, 250-350℃ and 450+℃. The total number of acid sites has been calculated at 0.368 mmol/g for the Ni-MMO support and 2.04 mmol/g for the molybdenum-doped MMO. The Mo-doped MMO demonstrated a sharper peak with a signal of 89 mV, an order of magnitude higher than the support, at 168℃. This was followed by a smaller secondary peak at 490℃ and ultimately indicates a significant presence of weaker acid sites which are active at lower temperatures following Mo-impregnation.

Comparatively, the $NiMo/Al_2O_3$ catalyst exhibited broader peaks over a greater temperature range indicating the presence of stronger acid sites. The $Pd_{1\%}/Al_2O_3$ material exhibited two smaller peaks at low temperatures, 163 and 273°C, before reaching a more significant and broader peak between 510 and 610°C, indicating the dominance of stronger Lewis acid sites. The $Pd_{2\%}$ and $Pd_{5\%}/Al_2O_3$ catalysts, exhibited a low intensity broad

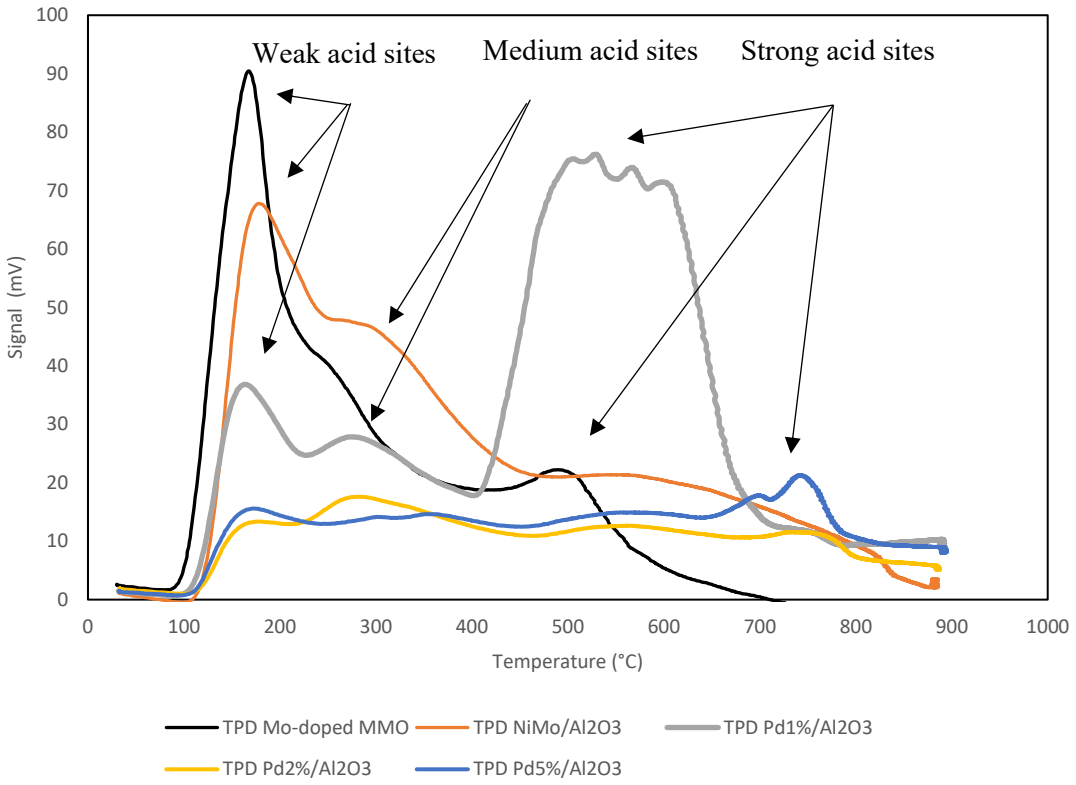

Figure 3. TPD profiles for the Mo-doped Ni-MMO species, $NiMo/Al_2O_3$ catalyst and $Pd_{1\%}$ - $Pd_{5\%}/Al_2O_3$.

peak ranging from 100 to 900°C, while the latter comprised a small peak at 744°C. For comparison, a γ-alumina catalyst bearing molybdenum, promoted by cobalt, exhibits a total acid site count of 1.513 mmol g^{-1} when using NH_3 as the adsorption agent [41].

Table 3 Acid site count using TPD NH_3

Catalyst	Acidity via NH_3 desorption (mmol g^{-1})
MMO support	0.368
Mo-MMO	2.04
$NiMo/Al_2O_3$	2.64
$Pd_{1\%}/Al_2O_3$	2.79
$Pd_{2\%}/Al_2O_3$	0.84
$Pd_{5\%}/Al_2O_3$	1.01

3.1.4 Morphology and metallic distribution

The images in Figure 4 (a-b) highlight the morphological structure of the heat-treated LDH structure. An approximation of the particle size pertains to approximately 200 nm crystallites. The plate-like agglomerates are typical of the rhombohedral crystallites in LDH-derived materials. The $NiMo/Al_2O_3$ image, Figure 4 (c), demonstrated less well-defined tubular morphology, approximating 50nm in length and 5nm in transverse length.

TEM imaging in Figure 4 (e) reveals the Al_2O_3 product in $Pd_{2\%}/Al_2O_3$ consists of disordered stacking nanofibers of length concentrating around 100nm, with a transverse width of less than 10nm. The $Pd_{1\%}/Al_2O_3$ morphology, shown in Figure 4 (d), demonstrates very similar attributes, approximating the same dimensions. The $Pd_{5\%}/Al_2O_3$, demonstrates a sphere morphology, the diameter of which does not generally exceed 10nm which can be observed in Figure 4 (f).

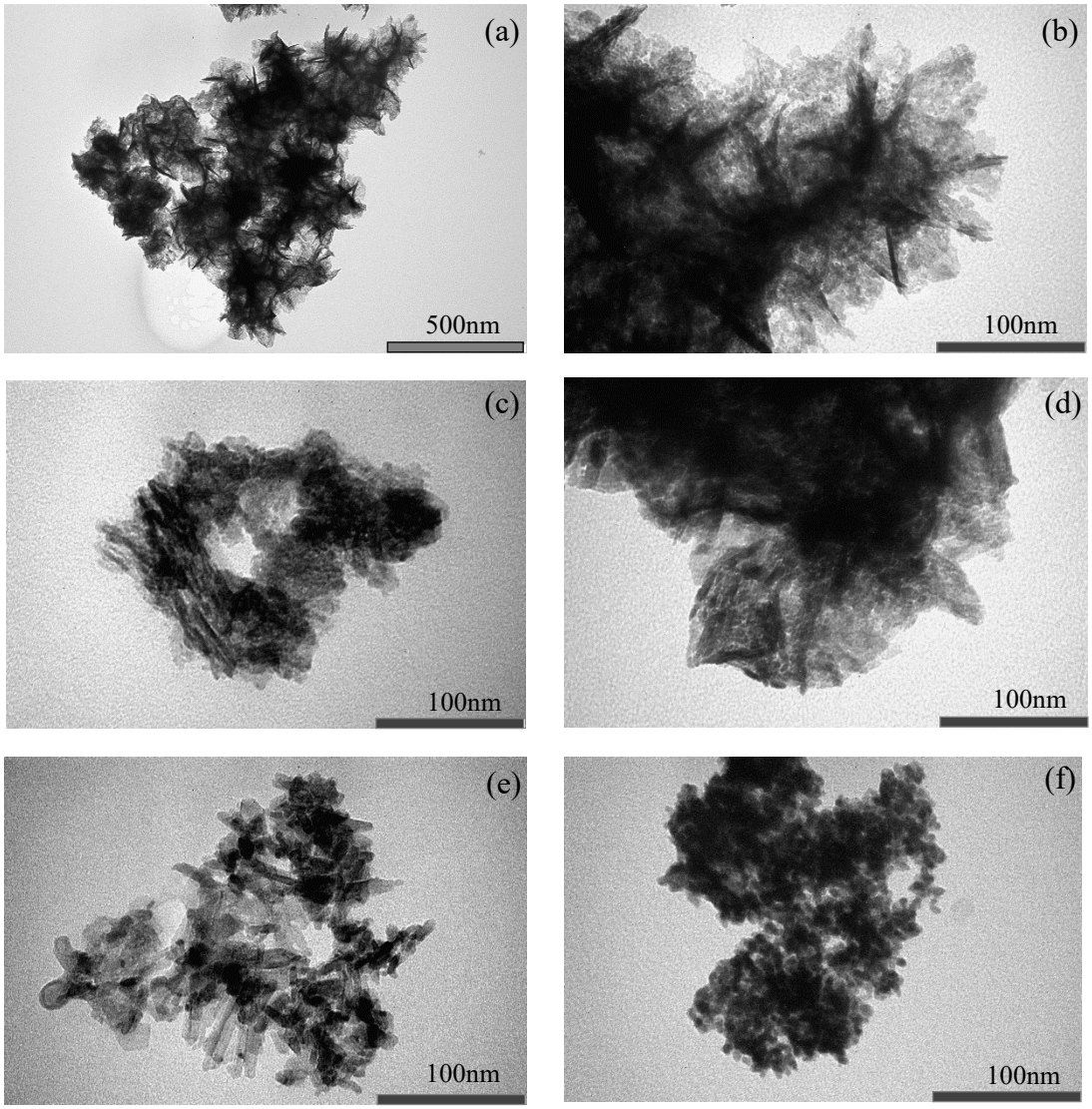

Figure 4. TEM imagery to elucidate crystal structure and shape (a&b) Mo-MMO (c) $NiMo/Al_2O_3$ (d) $Pd_{1\%}/Al_2O_3$ (e) $Pd_{2\%}/Al_2O_3$ and (f) $Pd_{5\%}/Al_2O_3$.

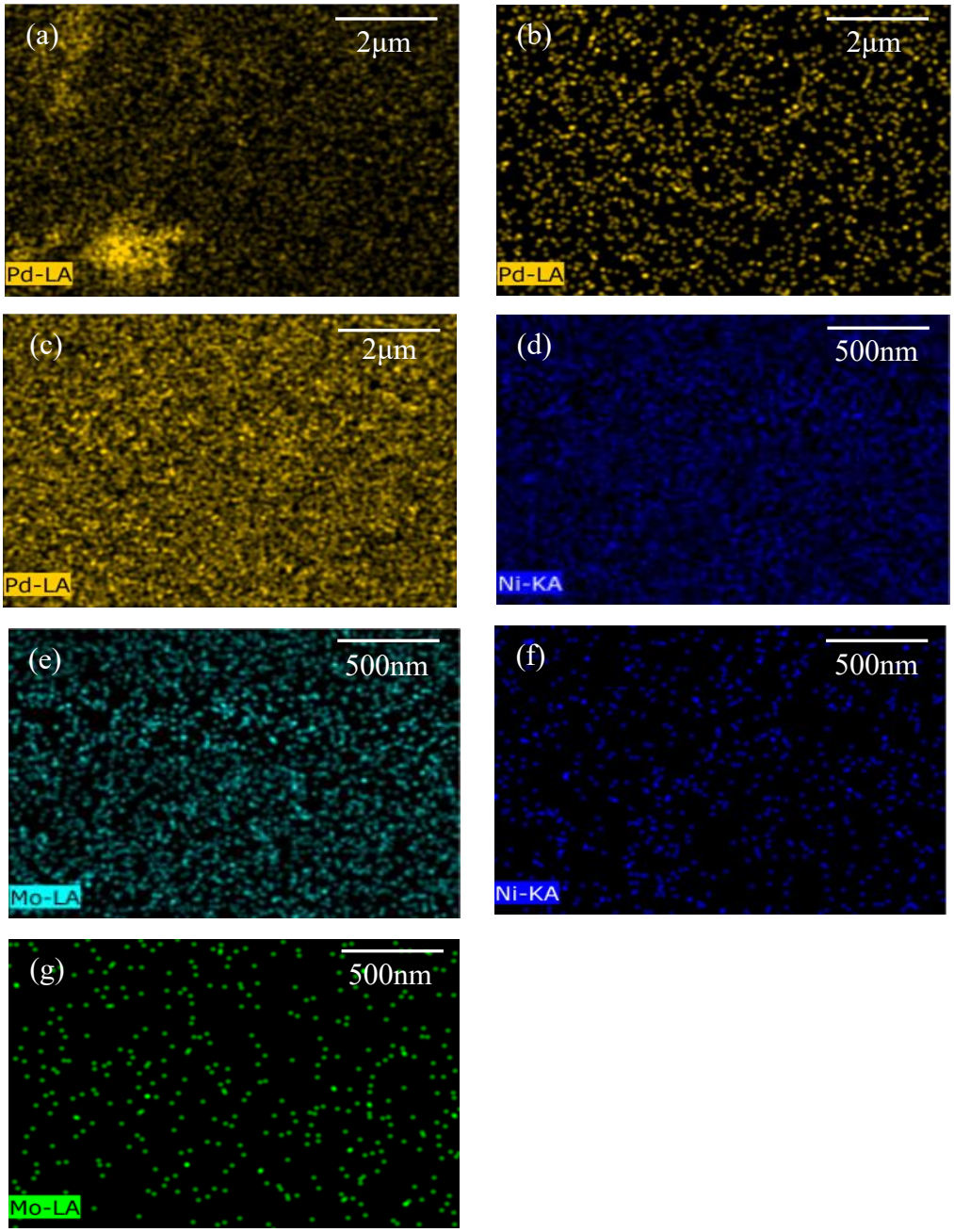

Figure 5. EDX analysis on the Pd/Al_2O_3 catalysts highlighting the distribution of Pd over the catalysts as a function of wt.% for (a) $Pd_{1\%}$/Al2O3 (b) $Pd_{2\%}/Al_2O_3$ and (c) $Pd_{5\%}/Al_2O_3$, in addition to the distribution of Ni and Mo over Mo-MMO (d&e) and $NiMo/Al_2O_3$ (f&g), respectively.

The EDS analysis of the Pd/Al_2O_3 catalysts clearly indicates the increased concentration of Pd deposited over the Al_2O_3 support as the loading increases. With $Pd_{1\%}/Al_2O_3$ in Figure 5 (a), the dispersion is not homogenous, rather areas of highly dispersed and agglomerated Pd exist, which is observed as random bright spots occupying the frame. As the concentration increases to $Pd_{2\%}$, as observed in Figure 5 (b), the Pd is more homogenous in its dispersion with higher density Pd epicenters deposited across the support. As the concentration increases to $Pd_{5\%}$ in Figure 5 (c), it is clear that again even richer epicenters of contiguous Pd exist, while the dispersion of the Pd is such that only a small fraction of the frame is Pd-deficient. This correlation may be linked to the sequential reduction in surface area exhibited by the catalysts with the trend as follows $Pd_{1\%}>Pd_{2\%}>Pd_{5\%}$, demonstrated in Table 2.

The distribution of Ni and Mo over the Mo-MMO and $NiMo/Al_2O_3$ catalyst show that the textural properties of anionic clay-derived MMO and Al_2O_3 supports affect the dispersion of the active species significantly. With the Mo-MMO support, the nickel is embedded as nickel oxides in a solid solution of both nickel and aluminum oxides making up the MMO. This leads to a more homogenous distribution, as highlighted in Figure 5 (d). The $NiMo/Al_2O_3$ catalyst is limited by both the concentration of nickel embedded on the support, as the content of nickel in the catalyst is comparatively lower, as well as the nature of its deposition through impregnation, subsequent to the preparation of the alumina support. As a result, Figure 5 (f), highlights the heterogenous dispersion with a lower Ni signal.

There is a clear difference in Mo distribution between the catalysts. As shown in Figure 5 (e), the distribution of the Mo is more homogenous over the Mo-MMO catalyst, while also exhibiting a comparatively higher signal. The heat treated anionic-clay-derived MMOs form large high surface area planar oxide layers with a more limited pore network as attested in Table 2. Consequently, it is expected that the Mo deposition is concentrated on the surface of the catalyst, while Mo incorporation into an Al_2O_3-supported catalyst, which is characterized

by a high pore volume and much greater surface area at 220.56 m^2 g^{-1}, will generate a greater distribution of internal Mo active centers not observed by the EDS analysis, hence the distribution of isolated Mo centers in Figure 5 (g).

3.2 Kinetic Study

Naphthalene undergoes partial hydrogenation to tetralin before complete hydrogenation to decalin, according to Scheme 1.

Scheme 1. Naphthalene hydrogenation reaction pathways.

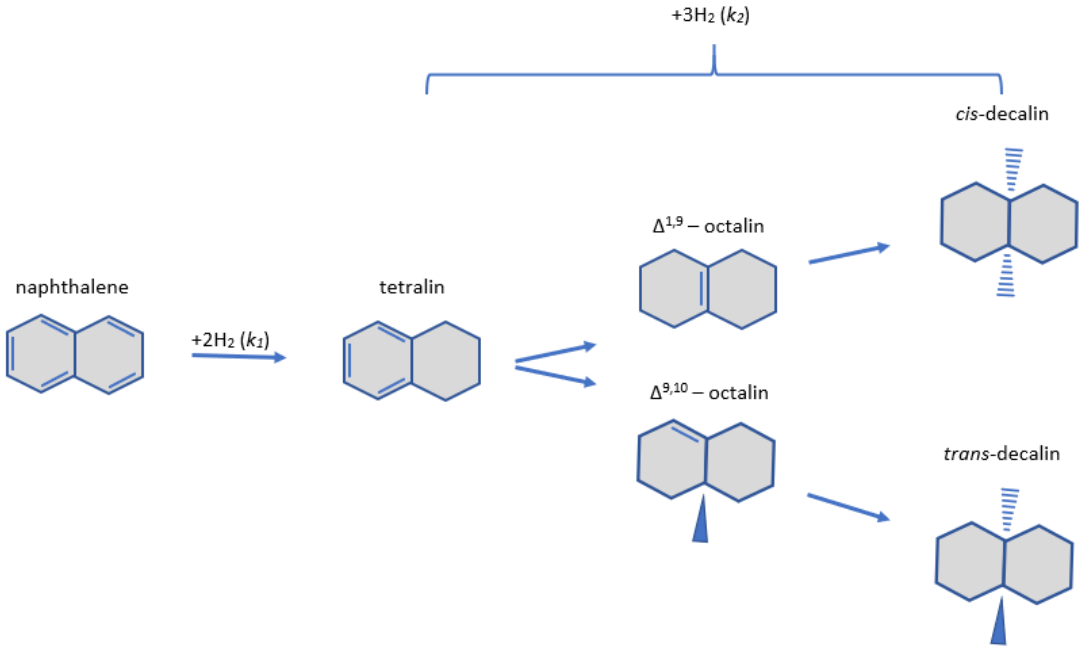

Decalin, however, comprises two particular isomers, cis- and trans-, where cis- is typically favored for improving the cetane number. The pseudo-first order model, used to derive values for k_1 and k_2, was selected as the enrichment of H_2 comprising the sole component in the reaction gas (H_2 >> Naphthalene) meant that it could be regarded as constant. Similar to previous works [13], the reaction mechanism can then be defined by the following set of equations:

$$[N] = [N_0] \times e^{-k_1 t} \quad (1)$$

$$[D] = [N_0] \times [1 + (k_1 e^{-k_2 t} - k_2 e^{-k_1 t})/(k_2 - k_1)] \quad (2)$$

$$[T] = [N_0] \times [1 + k_1 (e^{-k_1 t} - e^{-k_2 t})/(k_2 - k_1)] \quad (3)$$

where N, D and T stand for the naphthalene, decalin and tetralin concentrations, respectively; and N_0 is the naphthalene initial concentration. The reaction rate coefficients k_1 and k_2, shown in Table 4, were obtained simultaneously by minimizing the objective function, sum of squares of residuals (SSR), between the experimental and model-calculated naphthalene, tetralin and decalin concentration data points. The solver used was a non-linear Generalized Reduced Gradient (GRG) on Microsoft Excel.

The yields of naphthalene, tetralin and decalin for each catalyst regime are demonstrated in Figure 6. The experimental and modelling results are presented graphically in Figure 7 while the corresponding parity plots are shown in Figure 8.

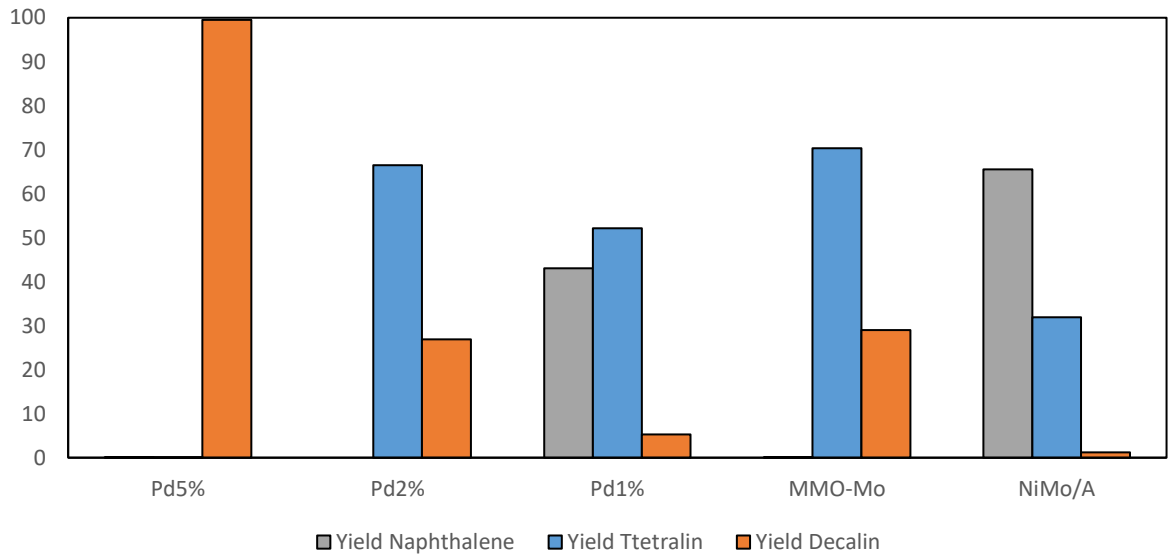

Figure 6. Yield of naphthalene, tetralin and decalin (cis & trans) for each catalyst regime.

In terms of the catalytic activity as shown in Figure 6, the $Pd_{5\%}/Al_2O_3$ catalyst is significantly more active than any of the other catalysts in the hydrogenation of naphthalene as can be observed by the conversion. This can be attributed to the both the comparatively high concentration of Pd deposited over the alumina, as well as the presence of contiguous Pd active sites which promote dissociative H_2 adsorption. $Pd_{5\%}/Al_2O_3$ achieves a yield of 99.5% decalin while as the concentration of the Pd loading decreases over the alumina support, so does the total decalin yield, to 26.9 and 5.3% for $Pd_{2\%}$ and $Pd_{1\%}/Al_2O_3$, respectively. While $Pd_{1\%}/Al_2O_3$ demonstrates a significantly higher proportion of acid sites as a result of the increased exposure of alumina acid sites, correlating with the increased surface area at 186.66 m2 g-1, it is clear that the hydrogenation of naphthalene is limited by the inhibited hydrogen adsorption facility of the catalyst with the lower concentration of Pd. The yields of decalin for the Ni and Mo-bearing catalysts at 29 and 1.2% for Mo-NiMMO and $NiMo/Al_2O_3$, respectively.

In terms of tetralin formation, the lowest yield follows the following trend: $Pd_{5\%}/Al_2O_3$ < Mo-NiMMO < $Pd_{2\%}/Al_2O_3$ < $Pd_{1\%}/Al_2O_3$ < $NiMo/Al_2O_3$. It is clear that the NiMo/ Al_2O_3 has the worst selectivity for the hydrogenation products after the reaction time. The majority of the product is naphthalene, whereas for all of the other catalytic regimes it is clear that either hydrogenation products, tetralin or decalin are favored. The only catalyst with a clear selectivity towards decalin products is the $Pd_{5\%}/Al_2O_3$.

When modelling according to pseudo-first order kinetics, k_1 and k_2 values were determined as shown in Table 4. The model used is presented graphically in Figure 7 in relation to the experimental results. The order of k_1 persists as follows: $Pd_{2\%}/Al_2O_3$ > $Pd_{5\%}/Al_2O_3$ > Mo-MMO > $Pd_{1\%}/Al_2O_3$ > $NiMo/Al_2O_3$. The order of k_2 values persists as follows $Pd_{5\%}/Al_2O_3$ > $Pd_{2\%}/Al_2O_3$ > Mo-MMO > $Pd_{1\%}/Al_2O_3$ > $NiMo/Al_2O_3$. As the Pd loading increases it would be expected that k_1 and k_2 values would increase, however, the reduction of k_1 values at a certain maximum contravenes this prediction.

Table 4 Calculated reaction rate constants, assuming pseudo-first order kinetics, for naphthalene conversion to tetralin and tetralin conversion to decalin, denoted k_1 and k_2, for

Catalyst	Pseudo-first order kinetic rate constant	
	k_1 (min^{-1})	k_2 (min^{-1})
$Pd_{5\%}/Al_2O_3$	0.0690	0.2240
$Pd_{2\%}/Al_2O_3$	0.1059	0.0031
$Pd_{1\%}/Al_2O_3$	0.0069	0.0012
$NiMo/Al_2O_3$	0.0036	0.0006
Mo-MMO	0.0353	0.0028

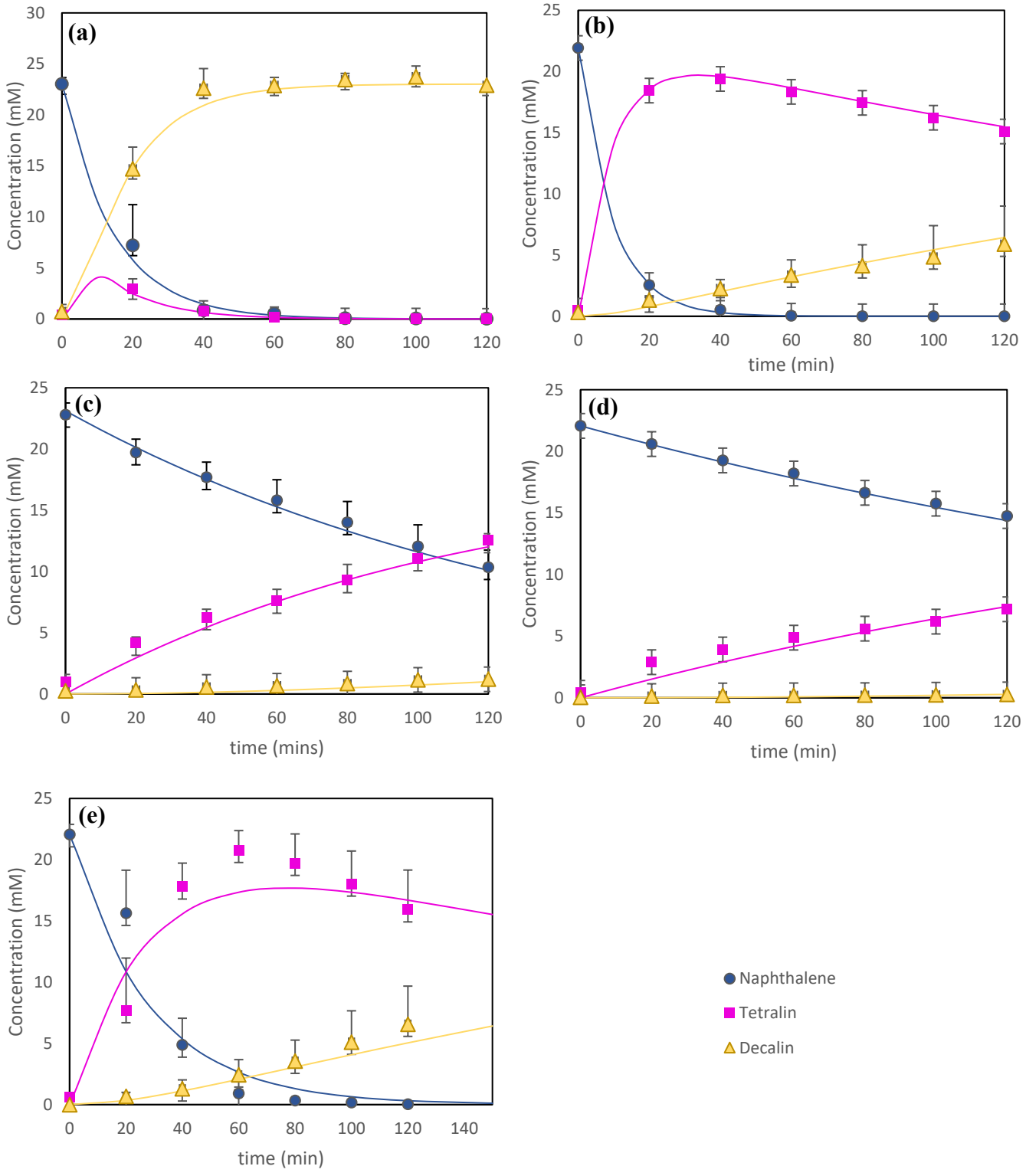

Figure 7. Plots of naphthalene, tetralin and decalin concentration against time using the experimentally-derived data and pseudo-first order kinetic model for each catalyst (a) $Pd_{5\%}$/alumina, (b) $Pd_{2\%}$/alumina (c) $Pd_{1\%}$/alumina (d) NiMo/alumina (e) Mo-MMO.

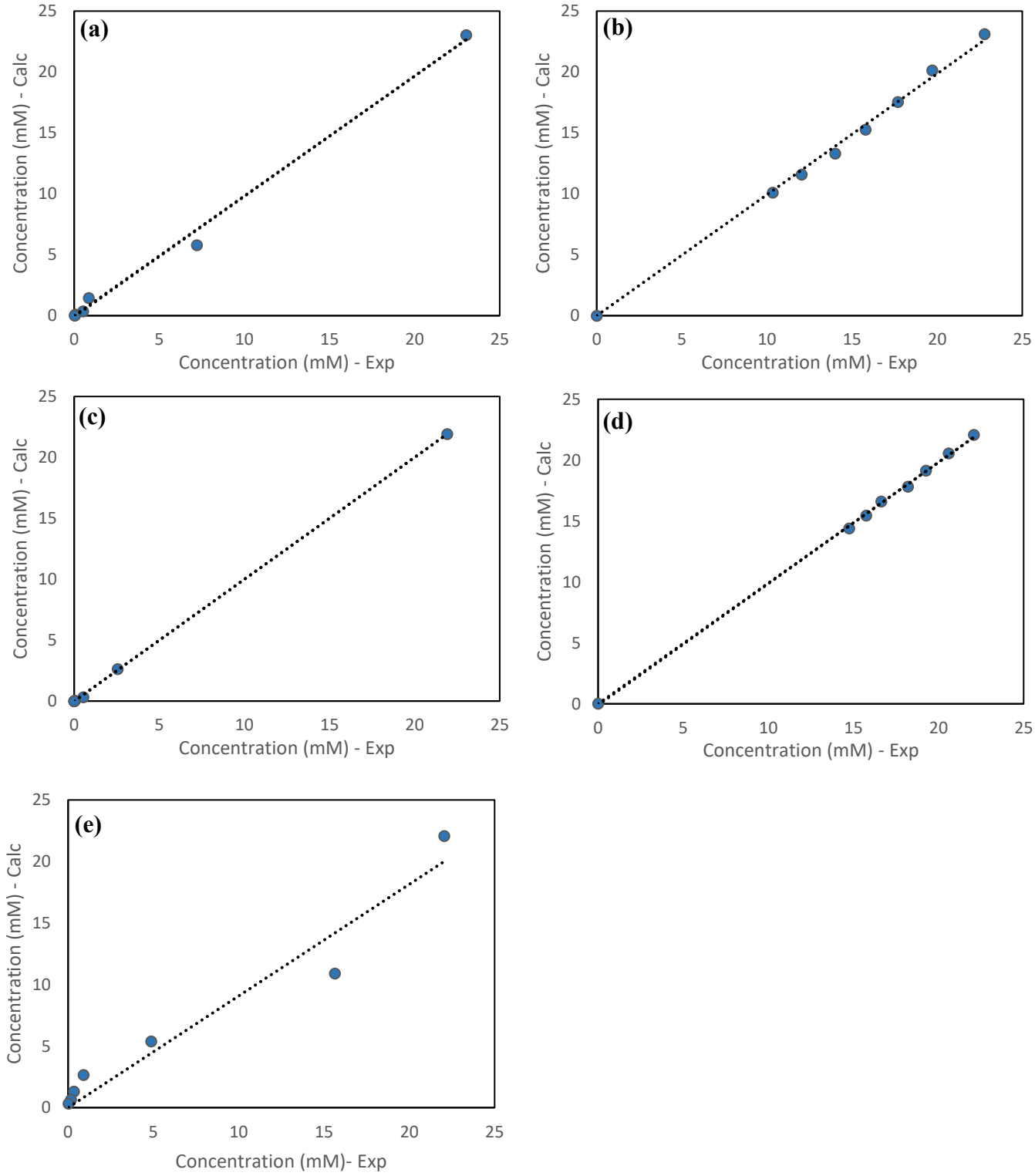

Figure 8. Parity plots for naphthalene concentration (a) Pd5%/alumina (b) $Pd_{2\%}$/alumina and (c) $Pd_{1\%}$/alumina (d) NiMo/alumina, and (e) Mo-MMO.

When using the $Pd_{5\%}/Al_2O_3$ coupled with this pseudo-first order reaction model, it becomes clear that the assumption of the second step being the rate determining step ($k_1 >> k_2$) does not hold. This is a detour from almost all conventional assumptions which also makes the simplified form provided in Escobar et al. [13], used for the platinum catalyst, non-applicable in this instance. It is clear that the advancement of catalytic activity provided by the $Pd_{5\%}/Al_2O_3$ is a superior material to be used in the more severe second-stage aromatic hydrogenation reactions. The results demonstrate that adsorption of tetralin is not a limitation with the abundance of palladium species on a $Pd_{5\%}/Al_2O_3$ under the reaction conditions used in this study. This therefore accelerates both cis and trans decalin formation and contradicts conventional k_1 and k_2 relationship assumptions. In addition, the calculated k_2 value is several orders of magnitude greater than the k_2 values for the lower concentration Pd species. The anticipated change in reaction rate constant follows a linear path in response to an increase in Pd concentration, given that the activation energy of the Pd over alumina species is expected to be constant. As a result, it is possible that the greater coverage of Pd over alumina which has generated a higher density of Pd clusters on the support, as seen in Figure 5 (c) derived from the EDS analysis, is impacting the electronic interactions on the surface of the catalyst. Coupled with the sphere-like morphology which generates a higher quantity of edge sites, exhibited by the $Pd_{5\%}$, demonstrated in Figure 4 (f) with a higher average pore size than the other catalysts demonstrated in Table 2, this has potentially provided the opportunity for tetralin to migrate to and bond with the active centers more readily. Competing against initial naphthalene molecules, tetralin can take advantage of greater dissociative adsorption for hydrogen activation, and subsequent conversion to decalin, as observed previously in Yu et al. [18]. As a result, it is suggested that the tetralin to decalin conversions is not structure-sensitive in the presence of $Pd_{5\%}$ dispersed over Al_2O_3.

While this confirms the advantage of a noble metal-enriched catalytic support in aromatic hydrogenation applications, the high cost and poor sulfur tolerance remains a significant drawback, particularly when dealing with sulfur-rich feeds typically observed in heavier oils. That said, when using $Pd_{1\%}/Al_2O_3$, the hydrogenation reaction proceeds at a much poorer rate with poor naphthalene conversion to tetralin, in addition to tetralin conversion to cis and trans decalin as shown in Figure 7 (c). The k_1 and k_2 values are one and two orders of magnitude lower than k_1 and k_2 for $Pd_{5\%}/Al_2O_3$, respectively.

In conventional catalytic regimes, the naphthalene to tetralin conversion is several orders of magnitude greater than the conversion of tetralin to the decalin isomers [23]. It has been suggested previously that when using a $NiMo/Al_2O_3$ catalyst, the strong adsorption of naphthalene on the active centers inhibits tetralin conversion to decalin until the naphthalene has been completely converted [42]. The Mo-MMO catalyst broadly concedes to this convention where after 120 min all of the naphthalene has been converted to tetralin whereas the tetralin has been unable to undergo complete conversion to decalin species, as observed in Figure 7 (e). However, it is noted that in this study, with the exception of $NiMo/Al_2O_3$ where an insignificant conversion of tetralin to decalin occurs, tetralin hydrogenation is simultaneously produced before naphthalene hydrogenation is completed. Accordingly, the data highlights k_1 values as an order greater than the k_2 values. As a result, the mechanism suggested by Su et al. [42] can be expanded upon. A distinctive difference in aromaticity prevalent between naphthalene and tetralin compounds results in a clear deviation to the hydrogenation reactivity when using a nickel-based catalyst. Tetralin exhibits a greater Pi-electron density than naphthalene which consequently generates a higher aromatic ring resonance energy. This higher energy inhibits hydrogenation reactivity when using non-noble metal species, leading to a strong discrepancy between k_1 and k_2 values. Furthermore, the difference in hydrogenation mechanisms of naphthalene and tetralin has been studied previously when in the presence of a Ni/Al_2O_3

catalyst [12]. While the weak aromaticity of naphthalene accommodates its conversion to tetralin under Pi/sigma adsorption which demands a single active site, the conversion of tetralin occurs through the Pi-adsorbed species, due its more potent aromaticity. It has previously been found that when using a Ni/Al_2O_3 catalyst, multiple Ni atoms are required to generate a tetralin hydrogenation active site and as a result the tetralin molecule can be considered catalyst structure-sensitive [12]. It may therefore be expected that the homogenous spread of Ni and Al in the MMO may promote more hydrogenation of naphthalene on the molybdenum oxide slabs, as compared to the $NiMo/Al_2O_3$ catalyst. A high conversion of naphthalene could then be responsible for the availability of the active sites to accommodate tetralin conversion, whereas in the $NiMo/Al_2O_3$ catalyst, the reduced dispersion due to the far lower concentration of the nickel promotor, as observed in the EDS analysis Figure 5 (f), will generate more isolated metallic active sites forming a bottle-neck in the reaction, leading to a reduced tetralin conversion and very limited decalin formation as observed in Figure 6, with a total decalin yield of 1.2%. While the textural characteristics of the $NiMo/Al_2O_3$ are more superior to the Ni-LDH-derived Mo species, as would be expected given the favorable properties of an alumina support, it is clear that the abundance and distribution of Ni, observed in Table 1 and Figures 5 (d&f), respectively, is the defining property in the hydrogenation reaction progression. It is evident that the Mo-MMO catalyst is more comparable to the $Pd_{2\%}$alumina, the latter's reaction progression of which is shown in Figure 7 (b), with a final yield of 29.0%. Comparatively, the activity of $NiMo/Al_2O_3$ is more comparable to $Pd_{1\%}/Al_2O_3$, though generates less tetralin and decalin than the $Pd_{1\%}/Al_2O_3$ catalyst.

In a previous study, it was concluded that the addition of a basic site-enriched catalyst support may augment the hydrogenation of naphthalene and tetralin, until a certain basic site concentration is reached whereupon the benefits are negated [13]. It is clear from the activity of tetralin conversion, variation in support materials which leads to variations in the electronic

configuration of the catalyst, that a distinct mechanism for the transformation of tetralin into its hydrogenated products is apparent between the catalyst regimes. To highlight these differences in catalytic activity and preferential pathways for tetralin hydrogenation, plots of cis/trans-decalin vs concentration of decalin formed were analyzed.

3.3 Cis/trans-decalin ratio

It is observed in Figure 9 (a) that when the Mo-MMO catalyst is used with the same catalyst to reactant ratio as the palladium-based catalysts, the cis/trans ratio begins at a comparatively high level compared to the other catalysts shown in both Figures 9 (a) and (b), at approximately 1.30. It begins to decline significantly as tetralin conversion to decalin ensues. However, when the basic site-enriched Mo-MMO support catalyst to reactant ratio is doubled to Mo-MMO double loading, for the same concentration of decalin, a greater concentration of trans-decalin is apparent initially with a cis/trans ratio of 0.32, and the trend is reversed leading to a gradual increase to 0.68 as the tetralin is converted. When using the acidic Al_2O_3-supported NiMo catalyst (used with double loading only), as shown in Figure 9 (c), the cis/trans ratio begins at 1.49 and gradually decreases with tetralin conversion to decalin, reaching a final ratio of 1.09. This trend is similar to that of the Mo-MMO single loading at the early tetralin conversion stage. When comparing the double loadings of $NiMo/Al_2O_3$ and Mo-MMO catalysts, the disparity between cis/trans ratio is clear. While the reaction has not proceeded to the same extent, it is clear that early conversion of the double loading Mo-MMO yields an enriched trans-decalin product in direct contradiction to $NiMo/Al_2O_3$. However, as tetralin conversion to decalin increases, so the concentration ratio appears to converge.

It has been postulated that the concentration of both the cis and trans isomers is dependent on two factors: (i) Isomerization activity of the catalyst and (ii) decalin-tetralin adsorption competition [15]. At low conversion of tetralin, the basic sites on the Mo-MMO catalyst are responsible for promoting isomerization to trans-decalin. There is however a significant

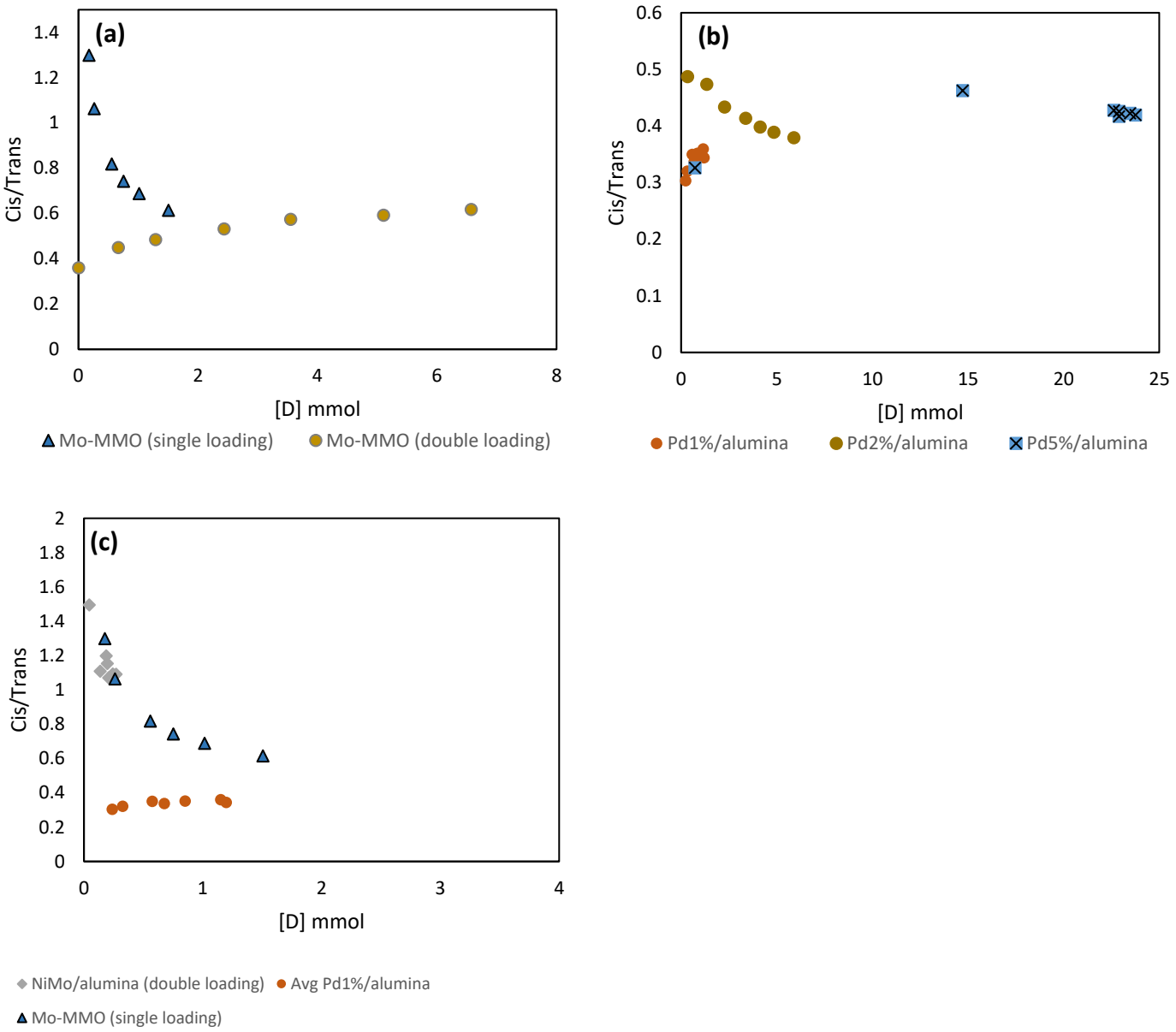

Figure 9. Plots of cis/trans ratio against decalin concentration for (a) two separate catalyst loadings of Mo-MMO and (b) including $Pd_{5\%}$/alumina, $Pd_{2\%}$/alumina and $Pd_{1\%}$/alumina and (c) NiMo/alumina, Pd-MMO, Mo-MMO (single loading) and $Pd_{1\%}$/alumina.

reduction in cis- isomerization to trans- decalin as the tetralin concentration decreases, after which the conversion stabilizes resulting in a trans-depleted decalin product with a 0.62 cis/trans ratio. The observed results agrees with Rautanen et al. [12] wherein long experiments resulting in poor tetralin conversion have resulted in an increase in cis-decalin. This is

exemplified with the Mo-MMO single loading and $NiMo/Al_2O_3$, observed in Figure 9 (c), wherein as the tetralin conversion slowly increases, rapid cis to trans isomerization takes place, particularly in the case of $NiMo/Al_2O_3$.

Furthermore, increases in competition for adsorption sites could greatly reduce the occurrence of the cis-trans isomerization reaction [15,43]. This is because although it has been previously reported that the cis to trans isomerization has a higher rate constant than tetralin hydrogenation, the tetralin molecules form a rigid parallel morphology against the surface of the catalyst compared to the hinged cis-decalin molecule [15]. This may explain the disparity between the single and double loadings of Mo-MMO, whereupon increasing the availability of adsorption sites, an increase in the cis to trans isomerization activity was observed i.e. the presence of tetralin was unable to block the active sites. This is also supported by the enhanced activity of cis to trans isomerization of Ni compared to Pd [15].

There is a clear difference between nickel and molybdenum-containing catalysts and the palladium bearing catalysts. With the latter, at both high concentration and low concentration on Al_2O_3, with both high and low conversion to decalin, the cis/trans ratio remains in favor of trans-decalin as highlighted in Figure 9 (b). The ratios for $Pd_{1\%}$, $Pd_{2\%}$ and $Pd_{5\%}$ end with 0.34, 0.38 and 0.42, respectively. This would suggest that there is a clear tendency to produce the trans-isomer under palladium irrespective of tetralin concentration. This corroborates with previous research which has shown that palladium occupies a higher trans-selectivity than its nickel-containing catalyst counterparts [12,15]. The comparative enrichment of trans-decalin, however, has been attributed to a very low intrinsic isomerization activity on the palladium catalyst which essentially stabilizes the produced cis/trans ratio throughout the entire tetralin conversion progression [15].

An underlying mechanism has been suggested by Dokjampa et al. [15], which speculates the cis/trans ratio is reliant on the orientation of the $\Delta^{1,9}$ – octalin intermediate. Hydrogen

incorporation into this octalin species is especially fast in the case of nickel catalysts, while the palladium catalyst accommodates a roll over on the surface, culminating in an orientation wherein the H atom in position 10 of the ring is facing away from the surface. This can be inferred considering the conformation of $\Delta^{1,9}$ – octalin on the catalyst surfaces; the syn nature of hydrogen addition requires the addition of H atoms to a double bond from the same side. Moreover, while the $\Delta^{9,10}$ – octalin exclusively produces cis decalin, the greater hydrogenation rate of $\Delta^{1,9}$ – octalin over noble metal catalysts, with the 10 atom facing away from the catalytic surface, greatly reduces isomerization to $\Delta^{9,10}$ – octalin resulting in a greater amount of trans-decalin production [12].

When using nickel and molybdenum catalysts, it is stipulated that the greater initial concentration of cis relative to trans is indicative of a preferred orientation of the $\Delta^{1,9}$ –octalin wherein the hydrogen atom in position 10 faces towards the surface. The addition of hydrogen atoms to positions 1 and 9 occurs on the same side thereby producing cis-decalin [15].

4. Conclusions

Mixed metal oxide carriers bearing a 3.3:1 Ni:Al ratio were synthesized from anionic clay species. The incipient wetness impregnation method was used to deposit molybdenum onto the surface of the support. The catalytic materials were tested in liquid-phase naphthalene hydrogenation at 250°C and 40 bar H_2. When comparing the Ni and Mo catalysts, the higher the loading of Ni present over the catalyst, the higher the conversion of naphthalene. It is also evident that when contrasting different Pd loadings over alumina, a higher loading of Pd produces a higher yield of decalin with the total yield ranging from 99.5 to 5.9% conversion for $Pd_{5\%}$ and $Pd_{1\%}$, respectively. Reaction rate constants were derived from a pseudo-first order kinetic pathway describing naphthalene to tetralin (k_1) and tetralin to decalin (k_2) hydrogenation. The Mo-MMO catalyst achieved comparable reaction rates to $Pd_{2\%}/Al_2O_3$ at double concentration, exceeding $Pd_{1\%}/Al_2O_3$, and $NiMo/Al_2O_3$. When using $Pd_{5\%}/Al_2O_3$,

tetralin hydrogenation was favored over naphthalene hydrogenation culminating in a k_2 value of 0.224 compared to a k_1 value of 0.069, detouring from the conventional assumption that $k_1 >> k_2$. The impact of catalyst on the cis/trans ratio against decalin concentration is clear. When using the Mo-MMO catalyst, the products initially contain a comparatively low cis-decalin concentration, followed by an inhibition of cis to trans isomerization and therefore a progressively more cis-decalin enriched product, mirroring that of the $NiMo/Al_2O_3$ catalyst. In comparison, the $Pd_{1\text{-}5\%}/Al_2O_3$ catalysts generate a much lower cis/trans ratio irrespective of tetralin concentration and palladium abundance, highlighting preferential for cis- to trans-decalin isomerization activity over Pd active sites. Consequently, NiMo-bearing catalysts, although offering poorer performance may provide greater advantages in simultaneous HYD and HDA processes due to cis-decalin's greater selectivity to indanes and alkyl-cyclohexanes. It is also evident that the enriched Mo-MMO offers benefits over the conventional refinery catalyst due to the comparative ease of synthesis of the LDH material in addition to more economic methods of formulation. Future work should include both the impact of sulfur on the hydrogenation process and catalyst performance, as well as hydrodecyclisation of the cis-decalin product to yield alkyl naphthenes.

5. Acknowledgements

The work contained in this paper was conducted during a PhD study undertaken as part of the Natural Environment Research Council (NERC) Centre for Doctoral Training (CDT) in Oil & Gas [grant number NEM00578X/1] and is funded by NERC and the School of Chemical Engineering at the University of Birmingham, whose support is gratefully acknowledged. The TPD analysis was performed by Dr. Helen Daly at the Department of Chemical Engineering and Analytical Science, University of Manchester. The BET analysis was conducted by Volkan Degirmenci, School of Engineering, University of Warwick.

6. References

1. Taillades-Jacquin, M.; Jones, D.; Roziere, J.; Moreno-Tost, R; Jiménez-López, A.; Albertazzi, S.; Vaccari, A.; Storaro, L.; Lenarda, M.; Trejo-Menayo, J. Novel mesoporous aluminosilicate supported palladium-rhodium catalysts for diesel upgrading. II. Catalytic activity and improvement of industrial diesel feedstocks. *Appl. Catal. A Gen.* **2008**, *340*, 257–264.

2. Mellios, G.; Kouridis, C. *Fuel quality in the EU in 2016*. 1st edition, Publications Office of the European Union: Luxembourg, 2018

3. Hart, A.; Leeke, G.; Greaves, M.; Wood, J. Down-hole heavy crude oil upgrading by CAPRI: Effect of hydrogen and methane gases upon upgrading and coke formation. *Fuel* **2014**, *119*, 226–235.

4. Bagci, S. A. Wet Forward Combustion for Heavy Oil Recovery. *Energy Sources, Part A Recover. Util. Environ. Eff.* **2006**, *28*, 221–232.

5. Elahi, S. M.; Ahmadi Khoshooei, L.; Carbognani, O.; Scott, C. E.; Chen, Z.; Pereira-Almao, P. Chemical insight into nano-catalytic in-situ upgrading and recovery of heavy oil. *Fuel* **2020**, *278*, 118270.

6. Chong, P.; Zhiming, Z.; Xiangchen, F.; Hualin, W. Thermodynamics and kinetics insights into naphthalene hydrogenation over a Ni-Mo catalyst. *Chinese J. Chem. Eng.* (2021) doi:10.1016/j.cjche.2021.02.007.

7. He, T.; Wang, Y.; Miao, P.; Li, J.; Wu, J.; Fang, Y. Hydrogenation of naphthalene over noble metal supported on mesoporous zeolite in the absence and presence of sulfur. *Fuel* **2013**, *106*, 365–371.

8. Jing, J. Y.; Yang, Z. F.; Wang, J.; Liu, D.; Feng, J.; Li, W. Effect of preparation methods on the structure and naphthalene hydrogenation performance of Ni2P/SiO2 catalyst. *Ranliao Huaxue Xuebao/Journal Fuel Chem. Technol.* **2020**, *48*, 842–851.

9. Prats, H.; Pinero, J. J.; Vines, F.; Bromley, S. T.; Sayos, R.; Illas, F. Assessing the usefulness of transition metal carbides for hydrogenation reactions. *Chem. Commun.* **2019**, *55*, 12797–12800.

10. Song, H.; Wang, J.; Wang, Z.; Song, H.; Li, F.; Jin, Z. Effect of titanium content on dibenzothiophene HDS performance over Ni 2P/Ti-MCM-41 catalyst. *J. Catal.* **2014**, *311*, 257–265.

11. Shen, Z.; He, P.; Wang, A.; Harrhy, J.; Meng, S.; Peng, H.; Song, H. Conversion of naphthalene as model compound of polyaromatics to mono-aromatic hydrocarbons under the mixed hydrogen and methane atmosphere. *Fuel* **2019**, *243*, 469–477.

12. Rautanen, P. A.; Lylykangas, M. S.; Aittamaa, J. R.; Krause, A. O. I. Liquid-phase hydrogenation of naphthalene and tetralin on Ni/Al2O3: Kinetic modeling. *Ind. Eng. Chem. Res.* **2002**, *41*, 5966–5975.

13. Escobar, J.; Barrera, M. C.; Santes, V.; Terrazas, J. E. Naphthalene hydrogenation over Mg-doped Pt/Al2O3. *Catal. Today* **296**, 197–204 (2017).

14. Rabl, S.; Haas, A.; Santi, D.; Flego, C.; Ferrari, M.; Calemma, V.; Weitkamp, J. Ring opening of cis-decalin on bifunctional Ir/- and Pt/La-X zeolite catalysts. *Appl. Catal. A Gen.* **2011**, *400*, 131–141.

15. Dokjampa, S.; Rirksomboon, T.; Osuwan, S.; Jongpatiwut, S.; Resasco, D. E. Comparative

study of the hydrogenation of tetralin on supported Ni, Pt, and Pd catalysts. *Catal. Today* **2007**, *123*, 218–223.

16. Wang, Q.; Hou, Y.; Zhao, H.; Li, Y.; Jia, A. Highly Selective Hydrogenation of Tetralin to cis-Decalin Using Ru Catalyst. *ChemistrySelect* **2019**, *4*, 5796–5798.

17. Lucci, F. R.; Darby, T. M.; Mattera, G. F. M.; Ivimey, J. C.; Therrien, J. A.; Michaelides, A.; Stamatakis, M.; Sykes, H. C. E. Controlling Hydrogen Activation, Spillover, and Desorption with Pd-Au Single-Atom Alloys. *J. Phys. Chem. Lett.* **2016**, *7*, 480–485.

18. Yu, W. Y.; Mullen, G. M.; Mullins, C. B. Hydrogen adsorption and absorption with Pd-Au bimetallic surfaces. *J. Phys. Chem. C* **2013**, *117*, 19535–19543.

19. Zhang, P.; Wu, T.; Hou, M.; Ma, J.; Liu, H.; Jiang, T.; Wang, W.; Wu, C.; Han, B. The hydrogenation of aromatic compounds under mild conditions by using a solid Lewis acid and supported palladium catalyst. *ChemCatChem* **2014**, *6*, 3323–3327.

20. Yoshimura, Y.; Toba, M.; Matsui, T.; Harada, M.; Ichihashi, Y.; Bando, K. K.; Yasuda, H.; Ishihara, H.; Morita, Y.; Kameoka, T. Active phases and sulfur tolerance of bimetallic Pd-Pt catalysts used for hydrotreatment. *Appl. Catal. A Gen.* **2007**, *322*, 152–171.

21. Bykov, A. V.; Alekseeva, D.; Demidenko, G.; Vasiliev, A.; Nikoshvili, L.; Kiwi-Minsker, L. New approach to synthesis of tetralin via naphthalene hydrogenation in supercritical conditions using polymer-stabilized PT nanoparticles. *Catalysts* **2020**, *10*, 1–14.

22. Wan, G.; Duan, A.; Zhao, Z.; Jiang, G.; Zhang, D.; Li, R.; Dou, T.; Chung, H. K. Al2O3-TiO2/Al2O 3-TiO2-SiO2 composite-supported bimetallic Pt-Pd catalysts for the hydrodearomatization and hydrodesulfurization of diesel fuel. *Energy and Fuels.* **2009**,

23, 81–85.

23. Kirumakki, S. R.; Shpeizer, B. G.; Sagar, G. V.; Chary, K. V. R.; Clearfield, A. Hydrogenation of Naphthalene over NiO/SiO2-Al2O3 catalysts: Structure-activity correlation. *J. Catal.* **2006**, *242*, 319–331.

24. Venezia, A. M.; La Parola, V.; Pawelec, B.; Fierro, J. L. G. Hydrogenation of aromatics over Au-Pd/SiO2-Al2O 3 catalysts; Support acidity effect. *Appl. Catal. A Gen.* **2004**, *264*, 43–51.

25. Navarro, R. M.; Pawelec, B.; Trejo, J. M.; Mariscal, R.; Fierro, J. L. G. Hydrogenation of Aromatics on Sulfur-Resistant PtPd Bimetallic Catalysts. **2000**, *194*, 184–194.

26. Lu, C. M.; Lin, Y. M.; Wang, I. Naphthalene hydrogenation over Pt/TiO2 - ZrO2 and the behavior of strong metal - Support interaction (SMSI). *Appl. Catal. A Gen.* **2000**, 198, 223–234.

27. Rodríguez-Castellón, E.; Diaz, L.; Braos-Garcia, P.; Merida-Robles, J.; Maireles-Torres, P.; Jimenez-Lopez, A.; Vaccari, A. Nickel-impregnated zirconium-doped mesoporous molecular sieves as catalysts for the hydrogenation and ring-opening of tetralin. *Appl. Catal. A Gen.* **2003**, *240*, 83–94.

28. Escobar-Alarcón, L.; Klimova, T.; Escobar-Aguilar, J.; Romero, S.; Morales-Ramirez, C.; Solis-Casados, D. Preparation and characterization of Al2O3-MgO catalytic supports modified with lithium. *Fuel.* **2013**, *110*, 278–285.

29. Caloch, B.; Rana, M. S.; Ancheyta, J. Improved hydrogenolysis (C-S, C-M) function with basic supported hydrodesulfurization catalysts. *Catal. Today.* **2004**, *98*, 91–98.

30. Fang, M.; Sánchez-delgado, R. A. Ruthenium nanoparticles supported on magnesium oxide : A versatile and recyclable dual-site catalyst for hydrogenation of mono- and. *J. Catal.* **2014**, *311*, 357–368.

31. Chen, W.; Nie, H.; Li, D.; Long, X.; Van Gestel, J.; Mauge, F. Effect of Mg addition on the structure and performance of sulfide Mo/Al2O3 in HDS and HDN reaction. *J. Catal.* **2016**, *344*, 420–433.

32. Albertazzi, S.; Busca, G.; Finocchio, E.; Glöckler, R.; Vaccari, A. New Pd/Pt on Mg/Al basic mixed oxides for the hydrogenation and hydrogenolysis of naphthalene. *J. Catal.* **2004**, *223*, 372–381.

33. Clause, O.; Coelho, G. M.; Gazzano, M.; Matteuzzi, D.; Trifiro, F.; Vaccari, A. Synthesis and thermal reactivity of nickel-containing anionic clays. *Appl. Clay Sci.* **1993**, *8*, 169–186.

34. Zhao, R.; Yin, C.; Zhao, H.; Liu, C. Synthesis, characterization, and application of hydotalcites in hydrodesulfurization of FCC gasoline. *Fuel Process. Technol.* **2003**, *81*, 201–209.

35. Kaur, G.; Couperthwaite, S. J.; Millar, G. J. Acid Mine Drainage Treatment Using Bayer Precipitates Obtained from Seawater Neutralization of Bayer Liquor. *Glob. Challenges* **2018**, *2*, 1800061.

36. Douglas, G. B. Contaminant removal from acidic mine pit water via in situ hydrotalcite formation. *Appl. Geochemistry.* **2014**, *51*, 15–22.

37. Álvarez, R.; Tóffolo, A.; Pérez, V.; Linares, C. F. Synthesis and characterization of

CoMo/Zn-Al mixed oxide catalysts for hydrodesulphuration of thiophene. *Catal. Letters* **2010**, *137*, 150–155.

38. Bennett, J. A.; Creamer, J. N.; Deplanche, K.; Macaskiy, E. L.; Shannon, J. I.; Wood, J. Palladium supported on bacterial biomass as a novel heterogeneous catalyst: A comparison of Pd/Al2O3 and bio-Pd in the hydrogenation of 2-pentyne. *Chem. Eng. Sci.* **2010**, *65*, 282–290.

39. Hart, A.; Omajali, B. J.; Murray, J. A.; Macaski, E. L.; Greaves, M.; Wood, J. Comparison of the effects of dispersed noble metal (Pd) biomass supported catalysts with typical hydrogenation (Pd/C, Pd/Al2O3) and hydrotreatment catalysts (CoMo/Al2O3) for in-situ heavy oil upgrading with Toe-to-Heel Air Injection (THAI). *Fuel.* **2016**, *180*, 367–376.

40. Cavani, F.; Trifirò, F.; Vaccari, A. Hydrotalcite-type anionic clays: Preparation, properties and applications. *Catal. Today.* **1991**, 11, 173–301.

41. Zarezadeh-Mehrizi, M.; Ebrahimi, A. A.; Rahimi, A. Comparison of γ and δ-Al2O3 supported CoMo catalysts in the hydrodesulfurization of straight-run gas oil. *Sci. Iran.* **2019**, *26*, 1555–1565.

42. Su, X.; An, P.; Gao, J.; Wang, R.; Zhang, Y.; Li, X.; Zhao, Y.; Liu, Y.; Ma, X.; Sun, M. Selective catalytic hydrogenation of naphthalene to tetralin over a Ni-Mo/Al2O3 catalyst. *Chinese J. Chem. Eng.* **2020**, *28*, 2566–2576.

43. Jongpatiwut, S.; Li, Z.; Resasco, E. D.; Alvarez, E. W.; Sughrue, L. E.; Dodwell, W. G. Competitive hydrogenation of poly-aromatic hydrocarbons on sulfur-resistant

bimetallic Pt-Pd catalysts. **2004**, *262*, 241–253.